Intersubband electron transitions due to electron-electron interactions in quantum-well structures

K. Kempa, P. Bakshi, J. Engelbrecht, and Y. Zhou
Department of Physics, Boston College, Chestnut Hill, Massachusetts 02467-3811
(Received 16 November 1999)

We have developed a full random-phase approximation formalism, and an efficient computational scheme for calculating the electron-electron scattering rates in quantum wells in nonequilibrium steady state, including the full dynamic screening. We apply our formalism to quantum-well systems studied in two recent experiments, which report different scattering rates for similar structures and similar carrier densities, and obtain quantitative agreement with both experiments. We show that the observed difference in the scattering rates is the result of different excitation levels in these experiments. We have also shown that the temperature dependence of the intersubband electron-electron scattering rate in one of the experiments is dominated by the higher-order, noncollective electron-electron scattering events at low temperature. We propose a scenario that could lead to the dominance of the electron-plasmon (collective) scattering processes. One of the experimental indications of this would be an activated temperature dependency of the intersubband electron-electron scattering rate.

The electron-electron scattering processes in homogeneous electron systems are well understood, at least in the random-phase approximation (RPA),[1] and this has provided a quantitative understanding of the mean free path of electrons in metals.[2,3] This is not the case in strongly inhomogeneous systems, even in those with the translational symmetry broken only in one dimension. Simplified approaches have been proposed[4,5] to treat such systems, which emphasize the single-particle (Auger) nature of the electron-electron scattering, but ignore[4] or phenomenologically approximate[5] the screening. A RPA-based approach, which includes effects of dynamical screening, was employed in Ref. 6 to study the relaxation of the nonequilibrium electron distribution function in a simple model quantum-well system.

Electron-electron scattering dominates the physics of carrier relaxation in quantum nanostructures for which the intersubband separation is less than the LO-phonon energy ($\sim$36 meV in GaAs). Knowledge of the electron-electron scattering rates is therefore crucial in determining the electrical and thermal transport properties of such structures. This is especially important for structures used as active regions of devices designed for emission of radiation in the THz frequency range.[7–9] Typically, these operate in a nonequilibrium steady state, and in some cases carry a large electron population in the active region. Then the electron-electron scattering becomes *the* limiting mechanism in achieving population inversion. Of obvious interest here is the possibility of reducing those electron-electron scattering rates (by appropriate structure design, or excitation scheme) so that a significant intersubband population inversion can be achieved.[9] This could clear the way to a THz laser.[9]

Experiments show that the intersubband electron-electron scattering rates in semiconductor quantum-well systems can be very high (of the order of 1 meV), almost approaching in some circumstances the intersubband scattering rate due to emission of LO phonons. However, two recent experiments,[10,11] performed on two-subband quantum-well structures (with the intersubband separation below the LO-phonon threshold), showed that the intersubband relaxation rates, due to electron-electron scattering, differed in the two experiments by over an order of magnitude even though the structures were similar, and had the same total electron density. An extension of the experimental scenario of Ref. 10, to include a detailed study of temperature and density dependence of the scattering rate, has been given in Ref. 12.

We present in this work a full RPA formalism, and an efficient calculational scheme, for the electron-electron scattering rate in quantum-well systems. This generalizes the previous efforts[4,5] and includes fully the dynamic screening via a detailed calculation based on the self-energy formalism. Such a complete treatment is essential for the proper justification of the calculational scheme. Our analysis is relevant for the nonequilibrium steady-state systems with significant carrier populations. We apply this formalism to the experimental scenarios of Refs. 10–12.

We consider here a nanostructure in which electrons are trapped, by an arbitrary confining potential, to a finite size domain in the z direction, and are free to move in any direction perpendicular to z. Assume, initially, that the energy spectrum consists of only two subbands. Since we are interested here in a nonequilibrium steady-state situation, we proceed as follows. First, we calculate the intersubband scattering rate for an equilibrium, nonzero temperature carrier distribution, using the Matsubara formalism.[1] Second (after performing all Matsubara summations), we identify the Fermion distribution functions with the state occupation factors. Finally, we employ these state occupation factors for the nonequilibrium steady state.

The averaged out scattering rate, $\gamma_{\rm scat}$, of an electron in the upper of the two subbands ($n=2$), can be obtained from the imaginary part of the corresponding self-energy, which in the RPA has the following form:[13]

$$\sum(\mathbf{r},\mathbf{r}',\omega_n)=\frac{1}{\beta}\sum_{\omega_m} S(\mathbf{r},\mathbf{r}',i\omega_m)G_0(\mathbf{r},\mathbf{r}',i\omega_n-i\omega_m) \tag{1}$$

where $\beta=1/kT$ and the Matsubara frequencies $\omega_m=2m\pi/\beta$, $\omega_n=(2n+1)\pi/\beta$, where n and m are integers. The noninteracting propagator is given by

$$G_0(\mathbf{r},\mathbf{r}',\omega)=\sum_{\mathbf{K}n}\frac{\Psi_{\mathbf{K}n}(\mathbf{r})\Psi^*_{\mathbf{K}n}(\mathbf{r}')}{\omega-E(\mathbf{K},n)+i\delta}, \tag{2}$$

where $\mathbf{K}$ is the electron, in-plane, wave vector, $n=1,2$ is the subband index, and $\mathbf{r}=(\mathbf{R},z)$, where $\mathbf{R}$ is the in-plane position vector. The single-particle energy is $E(\mathbf{K},n)=K^2/2m+\varepsilon_n$ (m is the effective mass, ε_n is the electron energy associated with the motion in z direction). In this paper we also set $\hbar=1$. $\Psi_{\mathbf{K}n}(\mathbf{r})$ is the corresponding single-particle eigenfunction of the state $\mathbf{K}$ in the nth subband. We employ the Lehman representation of the screened interaction:

$$S(\mathbf{r},\mathbf{r}',i\omega_m)=-\frac{1}{\pi}\int d\omega'\frac{\mathrm{Im}[S(\mathbf{r},\mathbf{r}',\omega')]}{i\omega_m-\omega'}. \tag{3}$$

The screened interaction $S(\mathbf{r},\mathbf{r}',\omega)$, is given in the RPA by the Dyson equation

$$S(\mathbf{r},\mathbf{r}',\omega)=v(\mathbf{r},\mathbf{r}')+\int d\mathbf{r}''\int d\mathbf{r}'''v(\mathbf{r},\mathbf{r}'')\times\chi_0(\mathbf{r}'',\mathbf{r}''',\omega)S(\mathbf{r}''',\mathbf{r}',\omega), \tag{4}$$

where the Coulomb potential is $v(\mathbf{r},\mathbf{r}')=e^2/\varepsilon|\mathbf{r}-\mathbf{r}'|$, where ε is the dielectric constant of the semiconductor, and the single-particle susceptibility is

$$\chi_0(\mathbf{r},\mathbf{r}',\omega)=\sum_{\mathbf{K}n}\sum_{\mathbf{K}'n'}\frac{(n_F[\mathbf{K},n]-n_F[\mathbf{K}',n']\Psi_{\mathbf{K}n}(\mathbf{r})\Psi^*_{\mathbf{K}n}(\mathbf{r}')\Psi^*_{\mathbf{K}n'}(\mathbf{r})\Psi_{\mathbf{K}n'}(\mathbf{r}')}{\omega+E(\mathbf{K},n)-E(\mathbf{K}',n')+i\delta} \tag{5}$$

with the Fermi distribution function given by $n_F[x]=1/(e^{x\beta}+1)$. The expectation value of the self-energy in the state $\mathbf{K},n$ is

$$D(\mathbf{K},n)=\int d\mathbf{r}\int d\mathbf{r}'\sum(\mathbf{r},\mathbf{r}',E[\mathbf{K},n])\Psi_{\mathbf{K}n}(\mathbf{r})\Psi^*_{\mathbf{K}n}(\mathbf{r}'). \tag{6}$$

Finally, the averaged scattering rate of an electron in the second subband is

$$\gamma_{\mathrm{scat}}=-2\langle\mathrm{Im}[D(\mathbf{K},2)]\rangle, \tag{7}$$

where $\langle\rangle$ denotes averaging over all states of the upper subband ($n=2$).

Performing the standard Matsubara summations, Fourier transforming the in-plane quantities using $[\exp(-i\mathbf{QR})]$, and employing the cosine Fourier transforms[14,15] along z, one can show that

$$\gamma_{\mathrm{scat}}=\left\langle-\frac{4}{\pi}\int\frac{d\mathbf{Q}}{(2\pi)^2}F(1,2,\mathbf{Q})\mathrm{Im}\{\Gamma_{1212}\}\right\rangle, \tag{8}$$

where

$$F(1,2,\mathbf{Q})=n_B[E(\mathbf{K},2)-E(\mathbf{K}+\mathbf{Q},1)]+n_F[-E(\mathbf{K}+\mathbf{Q},1)+\mu] \tag{9}$$

and $n_B[x]=1/(e^{x\beta}-1)$ is the Bose-Einstein distribution function with μ the chemical potential.
The interaction function Γ is defined as

$$\Gamma_{nn'mm'}=\int dq\int dq'S(q,q',\mathbf{Q},\omega)W_{nn'}(q)W_{mm'}(q') \tag{10}$$

with $W_{nn'}(q)=\int dz\cos(qz)\Psi_n(z)\Psi^*_{n'}(z)$. It is calculated by inverting the following matrix equation obtained from the transformed Dyson equation (4):

$$C_{mm'll'}=\sum_n\sum_{n'}\{\varepsilon\delta_{mm'nn'}-\chi_{nn'}(\mathbf{Q},\omega)C_{mm'nn'}\}\Gamma_{nn'll'} \tag{11}$$

in which n,n',m,m',l,l' are all either 1 or 2. Explicitly,

$$C_{mm'nn'}=B_{mm'nn'}-[Q/(2\pi e)^2]A_{mm'}A_{nn'}, \tag{12}$$

$$B_{mm'nn'}=\int dq\,v(q)W_{mm'}(q)W_{nn'}(q), \tag{13}$$

$$A_{mm'}=\int dq\,v(q)W_{mm'}(q), \tag{14}$$

where $v(q)=4\pi e^2/(q^2+Q^2)$. The transformed susceptibility function χ, which enters Eq. (11), is obtained by combining results of Refs. 15 and 16,

$$\chi_{nn'}(\mathbf{Q},\omega)=\frac{2mk_F}{\varepsilon_F^{1/2}\pi^2}n_F[E(\mathbf{K}n)]\times\sum_{s=-1}^{1}\frac{s}{2Q}\times\left[\int_0^\infty dk\,\frac{2\pi k}{\gamma\exp(k^2B)+1}\ln\left(\frac{k_s+k}{k_s-k}\right)\right], \tag{15}$$

where

$$k_s=\frac{1}{2Q}\{[E(\mathbf{K}n)-E(\mathbf{K}+\mathbf{Q},n')]s+(\omega+i\delta)-sQ^2\} \tag{16}$$

and $Q=|\mathbf{Q}|/k_F$, $\Omega=\omega/\varepsilon_F$, and $B=\beta\varepsilon_F$. The scaling factors are chosen to be the Fermi wave vector k_F, and the Fermi energy $\varepsilon_F=k_F^2/2m$, corresponding to the electron gas of the same density at $T=0$. γ is obtained from

$$\frac{3T^{3/2}}{2}\int_0^\infty du\ln[1+\gamma\exp(-u^2)]=1. \tag{17}$$

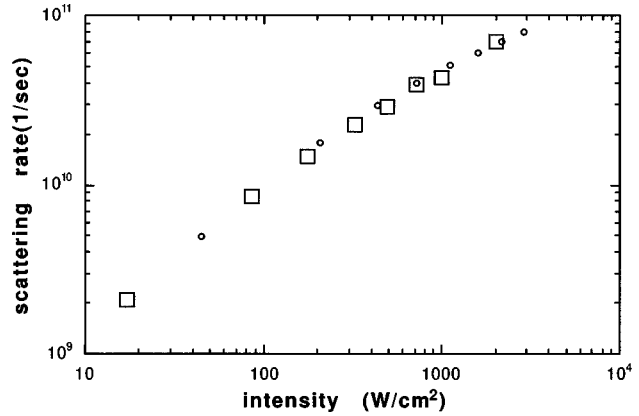

FIG. 1. Intersubband scattering rate vs intensity of the THz radiation. Circles represent our calculation and squares the experimental results of Ref. 10.

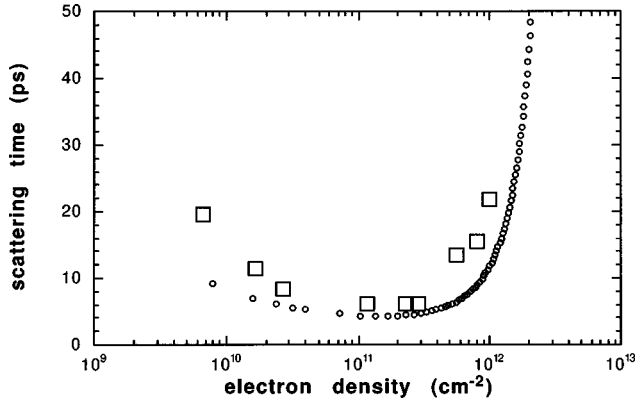

FIG. 2. Intersubband scattering time vs total electron density. Circles represent our calculation and squares the experimental results of Ref. 11.

Equation (11) can be easily solved by mapping of indices $nn' \rightarrow N$, $mm' \rightarrow M$, and $ll' \rightarrow L$, and subsequently by inverting the resulting (in the case of two subbands only) 4×4 matrix. The obtained Γ is used in the integrand of Eq. (8) to finally yield $\gamma_{\rm scat}$. An extension to multiple ($n>2$) subbands is straightforward, and amounts essentially to increasing the range of the subband summations.

To extend this formalism to the case of a steady-state nonequilibrium system, we first eliminate the Bose-Einstein distribution function from Eq. (9) by employing the identity

$$n_B[B-A](n_F[A]-n_F[B])=(1-n_F[A])n_F[B]. \quad (18)$$

Then, we substitute all of the Fermi distribution functions for the corresponding occupation factors, i.e., $n_F[E(\mathbf{K},n)] \rightarrow f(\mathbf{K},n)$.

In the experiments discussed below the scattering rate, averaged out over the states of a given subband, is measured for a given excitation condition. This justifies the averaging procedure employed in Eqs. (7) and (8), and also allows us to use, as a good approximation, the averaged out (over the nth subband) value of $f(\mathbf{K},n)$. Such an averaging procedure would be unjustified in the calculations (not performed here) of the nonequilibrium steady state, i.e., in calculations that aim at determining $f(\mathbf{K},n)$. Such calculations were performed in Ref. 6 by employing a formalism essentially similar to ours, combined with the transition rate balance equations.

We first apply our formalism to the experimental scenario of Ref. 10, where a double-well structure is remotely doped, so that electrons occupy the lower subband up to the Fermi level $E_{Fl}=4$ meV. A beam of THz radiation excites some of the electrons to the upper subband. The intersubband separation is $\Delta=11$ meV. All other subbands in this structure are at least 100 meV above this doublet. The occupation of the upper subband (N_2) is controlled by the radiation intensity (I), and can be estimated from the electron flux balance between the two subbands $N_1\gamma_{\rm THz}=N_2\gamma_{\rm scat}$, where N_1 is the lower subband population, and $\gamma_{\rm THz}$, proportional to I, is the upconversion rate due to the THz radiation. Figure 1 shows our calculation (circles) of $\gamma_{\rm scat}$ vs I compared with the experimental results (squares). The agreement is very good over the three orders of magnitude of I.

Next, we apply our formalism to a similar double-well, two subband structure of Ref. 11. In this case, a laser beam is used to excite electrons from the valence band into a narrow window which overlaps with both subbands in the conduction band. Since the excitation rate is very fast, the electron population divides, essentially equally (due to the constant density of states), between the two subbands. The final result of our calculation (circles) is shown in Fig. 2, and is in a good, quantitative agreement with the experiment (squares).

It should be emphasized that our calculations leading to the results shown in both Figs. 1 and 2 employed only parameters that were specified by the experimental scenarios. In the experiment of Ref. 10, for most of the radiation intensities, the electron gas had a smaller population in the upper band, compared to the case of the experiment of Ref. 11. Then, a simple phase-space blocking argument, combined with the quadratic scaling of the Auger process (pure two-particle, noncollective scattering) with the upper subband density, explains the smaller scattering rates measured in Ref. 10.

One of the results of the experiment reported in Ref. 10 was the temperature dependence of the intersubband scattering rate. It was suggested that $\gamma_{\rm scat} \sim A\exp(-E_{a1}/kT) + B\exp(-E_{a2}/kT)$, with the activation energy $E_{a1}=2.9$ meV for small temperature (T), and $E_{a2}=24$ meV for large T. While E_{a2} clearly is due to the emission of LO phonons ($\omega_{\rm LO}=\Delta+E_{a2}=35$ meV), the origin of the lower activation energy E_{a1} remained unexplained. In a later study,[12] this low-temperature domain was studied in detail. It was shown that the temperature dependency in this very low T range ($T<30$ K) is more complex than earlier suggested on the basis of a very limited number of data points. In fact, the scattering rate seems to follow T^2 dependency, in the temperature range $10\,{\rm K}<T<30\,{\rm K}$, before saturating at the level of $10^9\ {\rm sec}^{-1}$ for $T<10$ K (see Fig. 3, squares).

The results of our calculations ($\gamma_{\rm scat}$ vs T) for this case are shown in Fig. 3 (circles), together with the experimental results of Refs. 10 and 12 (squares). Our calculations agree well with the experiment in the window $10\,{\rm K}<T<30\,{\rm K}$. The higher *observed* scattering rates outside this range are due to mechanisms not included in our calculations (i.e., emission of LO phonons for $T>30$ K, and acoustic phonons for $T<10$ K). In Fig. 4 we separate the different contributions to

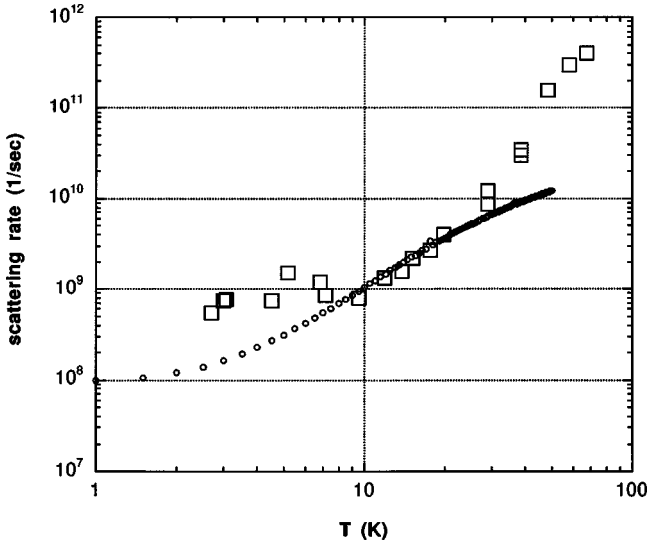

FIG. 3. Intersubband scattering rate vs temperature. Circles represent our calculation and squares the experimental results of Ref. 12.

our data in Fig. 3. The squares represent the full scattering rate, diamonds represent Auger scattering, i.e., due to the static screening obtained by setting S to v in the Dyson equation, and finally circles represent the difference between the two, i.e., scattering from plasmons and higher-order electron-electron processes. These results show that the low-temperature expansion for each of these curves is of the form $a+bT^2+\cdots$, where a for each curve represents a small residual scattering rate at $T=0$. In Fig. 4 this term has been subtracted for each curve. It is clear that for small T the *higher-order processes* contribute strongly to the scattering rate. The relative importance of these diminish for larger T. For the parameters of the experimental scenario of Ref. 12 (aerial density of $10^{11}\,\mathrm{cm}^{-2}$), however, even at $T=20\,\mathrm{K}$, they amount to 50% of the total scattering rate.

The T^2 scaling of the scattering rate is reminiscent of metallic behavior at low temperature,[17] and is entirely due to

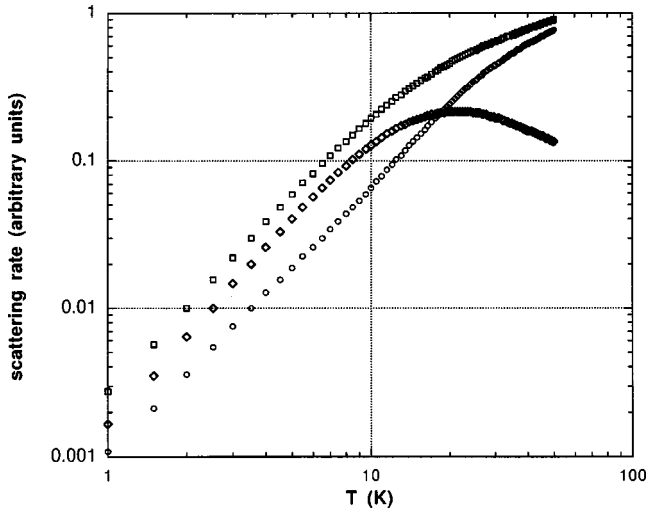

FIG. 4. Intersubband scattering vs temperature for calculation with all diagrams included (squares), including only the first RPA, ''ring,'' i.e., Auger processes (circles), and the contribution from all ''rings,'' except the first one (diamonds).

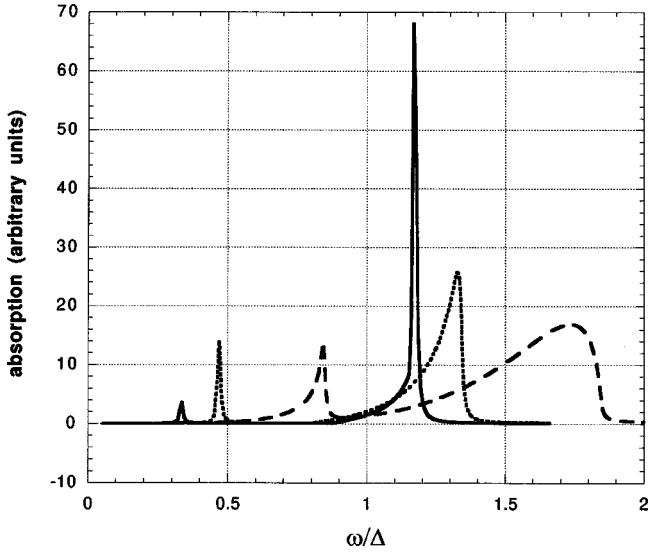

FIG. 5. Absorption spectrum vs normalized frequency ω/Δ. The solid line is for $q=0.3k_F$, dotted for $q=0.6k_F$, and dashed for $q=1.2k_F$.

the phase-space limitations on the allowed transitions. To relate this interpretation to our situation, we have calculated the absorption spectrum [$\sim \mathrm{Im}\,S(\omega,q)$]. We employed here the calculation scheme of Ref. 15. Figure 5 shows the absorption spectrum for three representative wave vectors q. The solid line shows that the spectrum for small q is dominated by collective excitations (the intrasubband and intersubband plasmons) which lie outside of the single-particle excitation continua. Note that the peaks are very narrow [the slight broadening is due to a small parameter $\delta=0.1\,\mathrm{meV}$, used in Eq. (5)], i.e., there is practically no Landau damping. This means that each electron has to be excited across a nonzero energy gap (of the order of the depolarization shift) to emit a plasmon. On the other hand, for larger q (indicated by the dotted and broken lines), the plasmon resonances enter the single-particle continua (note the large broadening of the plasmon peaks), and there is no need for an additional excitation of an electron to emit a plasmon (gapless situation). Since in the experimental scenario of Refs. 10 and 12, intersubband transitions from the upper band to the lower one can occur only for large q (small q transitions are phase-space blocked due to the large occupation of the lower subband), the gapless scenario dominates the physics. The upper band electrons therefore decay through the continuum of intermediate electron-hole states, as in the case of metals. This explains the T^2 dependency for all of the three curves shown in Fig. 4.

For the collective (plasma) effects to dominate the decay process, a scenario is needed which allows for downwards transitions with very small q. This will necessarily occur in structures, where a strong population inversion exists, i.e., the lower subband is essentially empty (see Refs. 9). In this case (see Fig. 5 for $q=0.3k_F$), the absorption spectrum will be dominated by the intersubband collective excitation (intersubband plasmon) which is separated from the edge of the single-particle continuum by a small gap E (of the order of the depolarization shift). We expect therefore an activated behavior of the scattering rates, i.e., given by a Boltzman factor $\gamma\sim\exp(-E/kT)$, in this case.

In conclusion, we have developed a full RPA formalism, and an efficient computational scheme for calculating the electron-electron scattering rate in semiconductor nanostructures, which includes fully the dynamical screening effects. Our calculations are in good quantitative agreement with recent experimental results, with no adjustable parameters. We have also shown that the temperature dependence of the intersubband electron-electron scattering rate in the quantum-well system of Refs. 10 and 12 is dominated by the higher-order electron-electron scatterings below $T=20\,\mathrm{K}$. We propose a scenario of strong population inversion that can be achieved in a wide class of structures, which leads to dominance of the electron-plasmon scattering. One of the experimental indications of this would be an activated dependency of electron-electron scattering.

We wish to thank K. Bedell, A. Nazarenko, and K. Unterrainer for helpful discussions. This work was supported by the U.S. Army Research Office under Grant No. DAAG55-97-1-0021.

[1] G. D. Mahan, *Many-Particle Physics* (Plenum, New York, 1990).
[2] C. Brundle, Surf. Sci. **48**, 99 (1975).
[3] L. Marton, J. Simpson, H. Fowler, and N. Swanson, Phys. Rev. **126**, 182 (1966).
[4] V. Fal'ko, Phys. Rev. B **47**, 13 585 (1993).
[5] P. Hyldgaard and J. Wilkins, Phys. Rev. B **53**, 6889 (1996).
[6] S. C. Lee and I. Galbraith, Phys. Rev. B **55**, R16 025 (1997).
[7] B. Williams, B. Xu, Q. Hu, and M. Melloch, Appl. Phys. Lett. **75**, 2927 (1999).
[8] M. Rochat, J. Faist, M. Beck, U. Oesterle, and M. Ilegems, Appl. Phys. Lett. **73**, 3724 (1998).
[9] K. Kempa, P. Bakshi, C. G. Du, G. Feng, A. Scorupsky, G. Strasser, C. Rauch, K. Unterrainer, and E. Gornik, J. Appl. Phys. **85**, 3708 (1999); P. Bakshi, K. Kempa, A. Scorupsky, C. G. Du, G. Feng, R. Zobl, G. Strasser, C. Rauch, Ch. Pacher, K. Unterrainer, and E. Gornik, Appl. Phys. Lett. **75**, 1685 (1999).
[10] J. N. Heyman, K. Unterrainer, K. Craig, B. Galdrikian, M. S. Sherwin, K. Campman, P. F. Hopkins, and A. C. Gossard, Phys. Rev. Lett. **74**, 2682 (1995).
[11] M. Hartig, S. Haacke, P. E. Selbmann, B. Deveaud, R. A. Taylor, and L. Rota, Phys. Rev. Lett. **80**, 1940 (1998); M. Hartig, J. D. Ganiere, P. E. Selbmann, B. Deveaud, and L. Rota, Phys. Rev. B **60**, 1500 (1999).
[12] J. N. Heyman, J. Barnhorst, K. Unterrainer, J. Williams, M. S. Sherwin, K. Campman, and A. C. Gossard, Physica E (Amsterdam) **2**, 195 (1998).
[13] J. C. Inkson, *Many-Body Theory of Solids* (Plenum, New York, 1984); R. D. Mattuck, *A Guide to Feynman Diagrams in the Many-Body Problem* (McGraw-Hill, New York, 1976).
[14] K. Kempa and W. L. Schaich, Phys. Rev. B **34**, 547 (1986).
[15] K. Kempa, D. A. Broido, C. Beckwith, and J. Cen, Phys. Rev. B **40**, 8385 (1989); K. D. Tsuei, W. W. Plummer, A. Liebsch, E. Pehlke, K. Kempa, and P. Bakshi, Surf. Sci. **247**, 302 (1991).
[16] J. Cen, Ph.D. thesis, Boston College, 1990.
[17] A. A. Abrikosov, L. P. Gorkov, and I. E. Dzyaloshinski, *Methods of Quantum Field Theory in Statistical Physics* (Dover, New York, 1963).